10

Model of Cell Membrane Electroporation and Transmembrane Molecular Transport

Damijan Miklavčič

Leila Towhidi*

10.1 Introduction

Electroporation is a technique in which, under the influence of electric field, the permeability of the cell membrane increases due to the formation of pores in the cell membrane, providing pathways for molecular transport (Abidor et al. 1979, Neumann et al. 1998, Tsong 1991, Weaver and Chizmadzhev 1989, Zimmermann 1982).

As electroporation is usually evaluated by indirect indications (Gehl and Mir 1999, He et al. 2008, Hibino et al. 1991, Kotnik et al. 2000, Neumann and Rosenheck 1972, Pavlin et al. 2007, Pliquett and Weaver 2007, Pucihar et al. 2007, Rols and Teissié 1998, Saulis 1997, Saulis et al. 2007, Schwister and Deuticke 1985), some experimental observations have not yet been fully explained. For instance, in a number of experiments using single-pulse electroporation protocol, increased conductivity and reduced transmembrane voltage were observed (Hibino et al. 1991, 1993), depending on the amplitude and duration of electric field (Kotnik et al. 2003, Rols and Teissié 1998). In multiple-pulse electroporation protocols, however, significant increase in cell molecular uptake is observed due to pulse fractionation, which, however, also depends on pulse repetition frequency. To explain these observations, knowing the exact mechanism of electroporation is crucial.

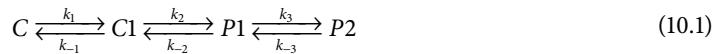* The work was done during her stay at the University of Ljubljana.

In spite of a wide use of electroporation with high reproducibility and effectiveness, the exact mechanisms of pore formation and closure, and, more importantly, resealing to membrane transport mechanism are not completely understood. Different theoretical models have been developed in order to interpret experimental results in a quantitative manner. Modeling, in addition to making the optimization of the process easier and reducing the experimental work and related costs, can serve as a test for our understanding of the mechanisms and processes behind the observed phenomena.

In this chapter, we present a *dynamic* model based on the reaction scheme used for pore formation and closure during and after the electric field exposure, while self-consistency is taken into account. In addition, by analyzing previously published experimental data (Glogauer et al. 1993, Puc et al. 2003, Pucihar et al. 2007, Rols et al. 1995, Zimmermann et al. 1990), we suggest two specific phenomena for resealing of the cell membrane—relaxation and memory effect (Teissié et al. 2005)—corresponding to two distinct transport processes: (1) interactive diffusion and (2) endocytotic-like transport. We investigated the number of loaded molecules to cells using our model. Simultaneously, the results of induced transmembrane voltage (*ITV*), the distribution of pores on the membrane surface, membrane conductivity changes, resealing behavior, and molecular uptake are obtained temporally and spatially. Using our model, we can describe and explain the results of single- and multiple-pulse electroporation protocols also taking into account pulse-repetition frequency and the number of pulses that has not been possible previously.

10.2 Model Descriptions

10.2.1 Membrane Structure and Conductivity Changes

When a cell is exposed to an external electric field, the *ITV* starts to increase based on the Laplace equation, which leads to the structural changes of the cell membrane. Based on a previously suggested (Neumann et al. 1999, Schmeer et al. 2004, Tsong 1991), and recently confirmed (Böckmann et al. 2008), kinetic model, in the first step the intact closed lipids (*C*) transform to tilted lipid head groups (*C1*). In the second step, the prepores (*P1*) are formed and, finally, in the last step, the final pores (*P2*) are formed. The sequential reaction can be described by Equation 10.1:

$$C \underset{k_{-1}}{\overset{k_1}{\rightleftharpoons}} C1 \underset{k_{-2}}{\overset{k_2}{\rightleftharpoons}} P1 \underset{k_{-3}}{\overset{k_3}{\rightleftharpoons}} P2 \qquad (10.1)$$

where *C1* is one intermediate closed or prepore state. The state *P1* denotes the pore structures of negligibly small permeability (transient or rapidly closing pore), while only *P2* is responsible for molecular uptake (stable or slowly closing pore). k_i and k_{-i} ($i = 1, 2, 3$) denote rate coefficients for pore formation and closure, respectively. For simplicity, the rate coefficients k_1, k_2, and k_3 are considered equal ($k_1 = k_2 = k_3 = k_p$) (Neumann et al. 1998). The rate laws for constituting steps in the scheme (Equation 10.1) are, respectively:

$$\frac{d\left[C(\vec{r},t)\right]}{dt} = -k_p\left[C(\vec{r},t)\right] + k_{-1}\left[C1(\vec{r},t)\right] \qquad (10.2)$$

$$\frac{d\left[C1(\vec{r},t)\right]}{dt} = -k_p\left(\left[C1(\vec{r},t)\right] - \left[C(\vec{r},t)\right]\right) - k_{-1}\left[C1(\vec{r},t)\right] + k_{-2}\left[P1(\vec{r},t)\right] \qquad (10.3)$$

$$\frac{d\left[P1(\vec{r},t)\right]}{dt} = -k_p\left(\left[P1(\vec{r},t)\right] - \left[C1(\vec{r},t)\right]\right) - k_{-2}\left[P1(\vec{r},t)\right] + k_{-3}\left[P2(\vec{r},t)\right] \qquad (10.4)$$

$$\frac{d\left[P2(\vec{r},t)\right]}{dt} = k_p\left[P1(\vec{r},t)\right] - k_{-3}\left[P2(\vec{r},t)\right] \qquad (10.5)$$

where

  t denotes time

  $\vec{r}$ is a vector representing the point on the membrane

  $[C]$, $[C1]$, $[P1]$, and $[P2]$ show the normalized distribution of each membrane lipid state to the initial value of closed state $[C(\vec{r},0)]$

Actually, $[C(\vec{r},0)] = [C_0]$ is a specific value for cell system under observation and is independent of field duration and strength (Neumann et al. 1998, 1999). In addition, at pulse switch-on time, the initial condition is $[C1(\vec{r},0)] = [P1(\vec{r},0)] = [P2(\vec{r},0)] = 0$. As demonstrated and discussed in the following sections, pore-formation-rate coefficient k_p depends on time and position on the membrane (i.e., it is field dependent), while the closure-rate coefficients (k_{-1}, k_{-2}, and k_{-3}) are constant (Gowrishankar et al. 1999, Neumann et al. 1998).

  The rate coefficients of the chemical-kinetics model can be described through equilibrium constant (K) by $K = k_i/k_{-i}$ (Kakorin et al. 1996). In the previous studies, the dependence of equilibrium constant in the membrane field (E_m) is given by the van't Hoff relationship (Kakorin et al. 1996). Using $E_m = ITV/d_m$, where d_m is the thickness of the membrane, the equilibrium constant can be obtained, using

$$K = K_0 \exp\left(\frac{\Delta V_p \varepsilon_0 (\varepsilon_W - \varepsilon_L)}{2 k_B T d_m^2} ITV^2 \right) \tag{10.6}$$

where

  K_0 is the value of K at $E = 0$

  ΔV_p is the mean volume change due to pore formation

  ε_0 is the permittivity of the vacuum

  ε_W and ε_L are the dielectric constants of water and lipids, respectively

  k_B is Boltzmann constant

  T is temperature

Whenever electroporation occurs, an increase in conductivity during the pulse is observed (Chernomordik et al. 1987, Glaser et al. 1988), which can be explained by the formation of pores in the cell membrane. Based on the trapezium barrier model for the image forces (Glaser et al. 1988, Kakorin and Neumann 2002), the intrinsic pore conductivities $\sigma_{p,i}$ ($i = 1$ and 2 represents $P1$ and $P2$ pores, respectively) are expressed as follows:

$$\sigma_{p,i} = \sigma_{p,i}{}^0 \exp\left(\alpha_{p,i} n |ITV| \frac{F}{RT} \right) \tag{10.7}$$

where

$$\sigma_{p,i}{}^0 = \frac{\sigma_{ex} + \sigma_{in}}{2} \exp\left(\frac{-\varphi_{im,i}{}^0 F}{RT} \right) \quad \text{and} \quad \alpha_{p,i} = 1 - \frac{RT}{F\varphi_{im,i}{}^0} \tag{10.8}$$

where

  σ_{ex} and σ_{in} are the extracellular and intracellular conductivities, respectively

  n is the geometrical parameter of the trapezium model for energy barrier (Kakorin and Neumann 2002)

  F is Faraday constant

  $\varphi_{im,i}{}^0$ is the intrinsic pore barrier potential

TABLE 10.1 Values of Parameters Used in the Simulations

Parameter	Symbol	Value	References
Membrane thickness	d_m	5e−9 m	Neumann et al. (1998)
Extracellular conductivity	σ_{ex}	0.14 S/m[a]	Neumann et al. (1998) and Pucihar et al. (2006)
Intracellular conductivity	σ_{in}	0.3 S/m[b]	Kotnik et al. (1998) and Neumann et al. (1998)
Initial conductivity of membrane	σ_{m0}	5e−7 S/m	Plonsey and Barr (1988) and Pucihar et al. (2008)
Extracellular permittivity	ε_o	7.1e−10 As/Vm	Neumann et al. (1998)
Intracellular permittivity	ε_i	7.1e−10 As/Vm	Neumann et al. (1998)
Membrane permittivity	ε_m	4.4e−11 As/Vm[c]	Neumann et al. (1998)
Water relative dielectric constant	ε_w	80 As/Vm	Neumann et al. (1998)
Lipid relative dielectric constant	ε_l	2 As/Vm	Neumann et al. (1998)
Free diffusion coefficient	D_0	5e−10 m²/s	Neumann et al. (1998)
Zero-field equilibrium constant	K_0	2e−2	Neumann et al. (1998)
Mean average aqueous pore volume	ΔV_p	9e−27 m³	Neumann et al. (1998)
Intrinsic barrier potential of P1 state	$\varphi_{im1}{}^0$	0.13 V	Kakorin and Neumann (2002)
Intrinsic barrier potential of P2 state	$\varphi_{im2}{}^0$	0.084 V	Kakorin and Neumann (2002)
A geometrical parameter	N	0.12	Schmeer et al. (2004)
Decay-rate coefficient for C1	k_{-1}	10^5 s⁻¹	Gowrishankar et al. (1999), Hibino et al. (1993), and Pucihar et al. (2002)
Decay-rate coefficient for P1 pores	k_{-2}	2000 s⁻¹	Bier (2002), Chernomordik et al. (1987), Gowrishankar et al. (1999), and Hibino et al. (1993)
Decay-rate coefficient for P2 pores	k_{-3}	2 s⁻¹	Chernomordik et al. (1987), Ghosh et al. (1993), and Gowrishankar et al. (1999), Neu et al. (1999)
Decay-rate coefficients for endocytotic-like process	k_f and k_s	0.044, 0.003 s⁻¹	Neumann et al. (1998)

[a] This is for spinner minimum essential medium (SMEM). The range of extracellular medium is quite large.
[b] Reported between 0.2 and 0.55 S/m.
[c] Reported between 4.4 and 5×10^{-11} As/Vm.

The values of constants are taken from related papers and given in Table 10.1.

Therefore, considering the normalized distribution of $P1$ and $P2$ pores, the initial (i.e., of nonelectroporated membrane) conductivity of membrane (σ_{m0}) and conductivity related to each kind of pores, the conductivity of membrane σ_m can be obtained as

$$\sigma_m(\vec{r},t) = \sigma_{m0} + \left[P1(\vec{r},t) \right] \times \sigma_{p,1} + \left[P2(\vec{r},t) \right] \times \sigma_{p,2} \tag{10.9}$$

10.2.2 Molecular Uptake

The experimentally obtained characteristic recovery times of the cell membrane fall into a wide range (Saulis et al. 1991). One reason for this wide range can be ascribed to different experimental methods that were used to obtain these data. The recovery time reported, based on measuring voltage and current (Bier 2002, Chernomordik et al. 1993, Ghosh et al. 1993, He et al. 2008), patch clamp (Ryttsén et al. 2000), ultrarapid video microscopy (Gabriel and Teissié 1999, Sowers 1986), and pulsed-laser fluorescence microscopy (Hibino et al. 1993, Kinosita and Ikegami 1988), is in the range of milliseconds. In studies based on finding the percentage of cells still incorporating various marker molecules at different times after electroporation (Glaser et al. 1986, Khine et al. 2007, Saulis 1997, Shirakashi et al. 2004, Teissié and Ramos 1998), the resealing time is reported to be about 20 min. Moreover, other experimental results were reported in which authors obtained the uptake of particular marker molecules under conditions when marker molecules were either present or absent at the time of cell exposure

to electric pulses. It was demonstrated that in the case of the probe presence at the pulse time, probe entrance to cells was uniform, whereas it was localized in large vesicles when the probe was added after the exposure (Glogauer et al. 1993, Rols et al. 1995, Zimmermann et al. 1990). In addition, the internalized components of the membrane after electroporation were observed (Glogauer et al. 1993). The authors suggested that in addition to passive diffusion through pores, an endocytosis-like (or macropinocytosis-like) transport also partially contributes to the loading of the molecule after the pulse at the electroporated area of membrane. This mechanism was suggested to occur due to the initiation of the membrane ruffling after the electroporation (Escoffre et al. 2007, Jones 2007, Lambert et al. 1990). The very short characteristic time of resealing for artificial lipid membranes (in the range of microseconds and millisecond), compared to biological cells (in the range of hours) (Glaser et al. 1986, Navarrete and Sacchi 2006), supports the involvement of the suggested endocytosis-like transport.

Based on the above considerations, we define two transport mechanisms: the first one is transport through the created pores on the membrane with relatively fast relaxation due to pore closure, and the second one is transport due to enhanced membrane perturbation and ruffling with quite slow resealing (Glogauer et al. 1993). The attributed mechanisms for uptake in each mentioned case are suggested to be interactive diffusion (Neumann et al. 1998) and endocytotic-like transport, respectively, which will be explained further in following sections.

10.2.2.1 Pores and Interactive Diffusion

It is believed that there are three mechanisms involved in molecular transport through the pores: diffusion, electrophoresis, and electroosmosis. Because of a short duration of electric pulses, diffusion is considered to be the predominant transport mechanism for small molecule cell uptake (Prausnitz et al. 1995, Puc et al. 2003).

From Equation 10.9 it can be seen that membrane conductivity changes depend on both P1 and P2 pores; therefore, the closure of pores is responsible for decreasing the conductivity of the membrane after the pulse. Due to the transient contacts of the molecule with the lipids of the pore edges, the transport of molecules through the membrane in this case is not free diffusion but interactive diffusion, which is reflected in diffusion coefficient with slightly lower value than free diffusion coefficient (Neumann et al. 1998). We should also consider that membrane conductivity is decreased in part also by this interactive diffusion as pores are occluded by molecules being transported through the pores.

10.2.2.2 Perturbed Area and Endocytotic-Like Transport

Although a strong decrease in the flow of molecules was seen shortly after the pulse (Gabriel and Teissié 1999), the observed increased membrane permeability is a long-lasting phenomenon (Glaser et al. 1986, Neumann et al. 1998, Saulis 1997, 2005, Teissié and Ramos 1998). In our study, this long-lasting phenomenon corresponds to the perturbed area of the membrane and is assigned to endocytosis-like transport, which has already been suggested previously (Glogauer et al. 1993, Rols et al. 1995, Zimmermann et al. 1990). Memory effect resealing in some studies was observed to fit simple exponentially decaying function (Rols and Teissié 1990) or a more complex exponential behavior (Glaser et al. 1986, Khine et al. 2007, Neumann et al. 1998, Pucihar et al. 2008). In our model, we considered a dual exponential decay function for returning the cell membrane to its normal state:

$$[M] = [P2]_e \left(B \exp(-k_f t) + (1-B) \exp(-k_s t) \right) \tag{10.10}$$

where

$[M]$ shows the normalized distribution of perturbed area due to electroporation
$[P2]_e$ is the normalized distribution of pores at the end of pulse
k_f and k_s are decay-rate coefficients for endocytotic-like transport
B is a constant

k_f, k_s, and B are obtainable from the experimental results and depend on the type and size of transported molecules (Neumann et al. 1998).

10.2.2.3 Transmembrane Molecular Transport

In our model, two different transport coefficients are assigned to two transport mechanisms (interactive diffusion and endocytotic-like transport). With respect to these, the permeability of the membrane can be written as the sum of two distinct contributions:

$$P_m(\vec{r},t) = \frac{\left[P2(\vec{r},t) \right] D_p}{d_m} + \frac{\left[M(\vec{r},t) \right] D_r}{d_m} \qquad (10.11)$$

where D_p and D_r are the diffusion coefficients for interactive transport and transport coefficient related to endocytosis-like transport, respectively.

It should be noted that D_p is about 0.1–0.3 of the free diffusion coefficient D_0 (depending on the type of molecule passing through the membrane) (Neumann et al. 1999, Pavlin et al. 2005), whereas D_r has been assigned a very low value (about $D_0/10,000$) (Neumann et al. 1999).

While the membrane is being permeabilized due to electric field, the molecules pass through the membrane based on concentration gradient. A quantitative description of diffusion is contained in Fick's first law (Plonsey and Barr 1988). The flux through the cell membrane (j) can be approximated by $j = P_m(c^{out} - c^{in})$, where c^{out} and c^{in} are the outside and inside concentrations adjacent to the membrane, and P_m is membrane permeability coefficient as described in Equation 10.11. In order to obtain the total moles transported to the cell (N_{mol}), an integration of j over the surface and time is performed as

$$N_{mol} = \int_{t=0}^{\tau} \int_S j \, dS \, dt \qquad (10.12)$$

where
  S is the surface of the cell membrane
  τ is the time at which the quantity of transported molecules is to be determined.

The number of molecules transported through the membrane (N) can be then obtained by $N = N_A N_{mol}$.

10.3 Construction of the Model

The simulations in this study were performed using COMSOL 3.3 package (COMSOL Inc., Burlington, Massachusetts) based on finite element method. In order to construct a favorable geometrical model, a spherical cell with a radius of 5.6 μm was located inside a cylinder. The two circular electrodes were positioned at the bases of the cylinder, which are shown shaded in Figure 10.1A. The cylinder was chosen to take advantage of symmetry for simplifying the 3D geometrical model to a 2D-axial symmetry, and therefore saving time and memory during simulations (Figure 10.1B). With the purpose of complying with reality, the applied voltage to the electrodes was considered as a smoothed step function with the rising and falling times of 2 μs.

Incorporating extremely thin membrane compared to the cell size is problematic in meshing and solving the problem. Therefore, we assigned boundary condition to the membrane as previously described (Pucihar et al. 2006). In our calculations, the resting voltage was considered to be negligible with respect to the *ITV*.

The interactive diffusion coefficient was taken to be $D_p = D_0/5$, and the attributed transport coefficient to induced endocytosis-like transport process was set to $D_r = D_0/10,000$ (Neumann et al.
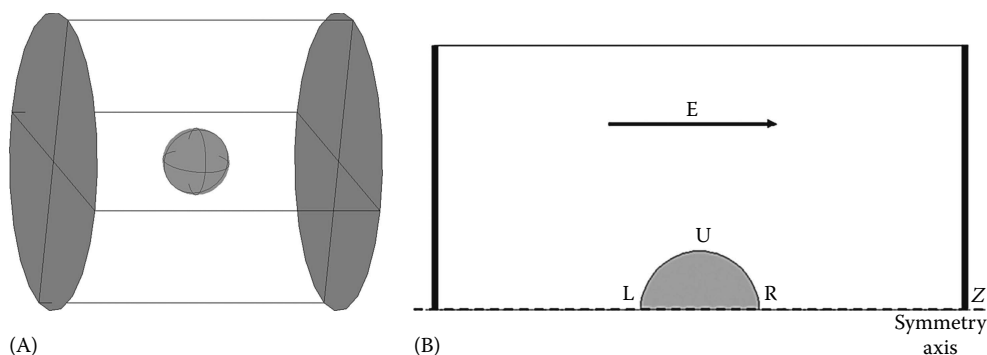
FIGURE 10.1 Simulation geometrical model. Schematic of a spherical cell placed between electrodes. The cell and electrodes are shaded. (A) 3D geometry. (B) Simplified 2D axial symmetry of the model with dashed line as the symmetry axis. The right pole, left pole, and the upper equator are indicated by R, L, and U, respectively. The arrow denotes the direction of the electric field.

1999) for a typical molecule (e.g., Serva Blue G). It is obvious that this value depends on the size and type of transported molecules through the transporting pathways of the membrane. The initial concentrations of intracellular and extracellular probe were set to be 0 and 10 mM, respectively, and the temperature was considered to be 20°C. As the changes near the membrane are more pronounced and important, we increased the number of meshing elements for finite element solver at these regions. Our simulation was designed to solve the Laplace equation in the region between two electrodes containing the cell to obtain the *ITV*, considering all the adjoined equations in this model. This set of equations should be solved for *ITV* and membrane conductivity, considering self-consistency of the parameters. In other words, as the unknowns are tightly involved, these equations should be solved simultaneously. The total number of internalized molecules to the cell in our model was obtained by integrating all the transported molecules from the entire cell membrane area for about 1000 s (i.e., approximately 20 min) after the pulse, after which the transport of molecules across the cell membrane becomes negligible.

The necessary parameters and the reference sources used for the simulation are listed in Table 10.1. All the simulations were performed on a PC equipped with a 2.8 GHz Pentium IV processor and 3 GB RAM. Each simulation run lasts between about 1 and 10 min, depending on the number of pulses and the elapsed time after the exposure of the cell to the electric field. Following the simulations, all the spatial and temporal quantities related to membrane conductivity, *ITV*, concentration, and molecular uptake are available.

10.4 Results

10.4.1 Structural Changes in the Membrane

After the start of the pulse, structural alterations in the form of pore formation start to appear without any threshold being imposed explicitly (Figure 10.2). The results for distribution of structural changes related to P1 and P2 pores on the cell membrane surface at the end of the pulse with three different field strengths and 100 μs duration are shown in Figure 10.2A and B. It is evident that in the cap regions (L and R in Figure 10.1), in which *ITV* is higher, pore formation is most pronounced. It can also be observed that the pore formation at 600 V/cm is negligible compared to the higher values of 800 and 1000 V/cm.
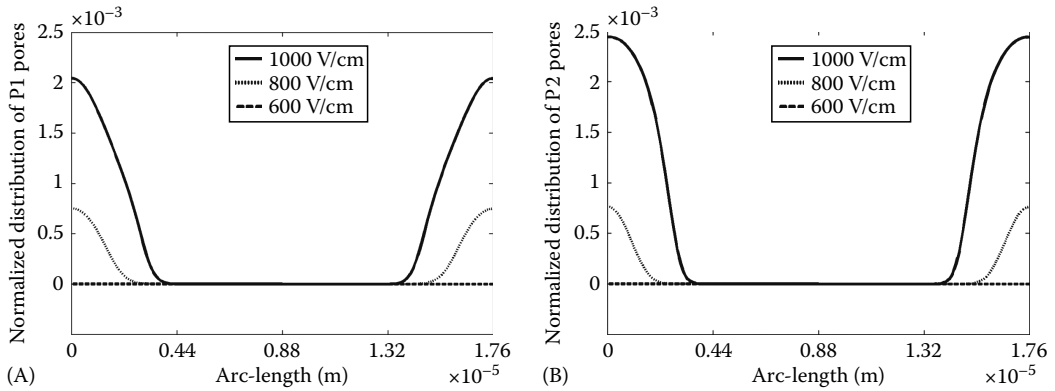
FIGURE 10.2 Normalized distribution of pores on the membrane. Normalized distribution of (A) P1 pores and (B) P2 pores on the cell membrane at the end of pulses of 600, 800, and 1000 V/cm with duration of 100 μs. The right pole, left pole, and the upper equator are indicated by R, L, and U, respectively.

10.4.2 Membrane Conductivity

Figure 10.3A displays the temporal membrane conductivity averaged over the cell membrane during 100 μs pulses considered in Figure 10.2 (considered voltages were 600, 800, and 1000 V/cm). It can be observed that the conductivity increase due to applied 600 V/cm is very small. Membrane conductivity related to 1000 V/cm first increases sharply, then a much slower increase is observed. At the end of pulse, the membrane conductivity is increased by a factor of 1000. The overall conductivity starts to disappear after the pulse termination (Figure 10.3B).

The effect of pulse duration on membrane conductivity increase for a 1000 V/cm pulse can be observed in Figure 10.3C. This figure reveals that the longer the pulse, the more efficient electroporation.

10.4.3 Induced Transmembrane Voltage

After the smoothed-step pulse is switched on, the membrane as a capacitor starts charging and *ITV* starts to increase that in turn results in membrane conductivity increase (Figure 10.3A). In some cases, even a decrease of the *ITV* value may be observed as a dip at poles (Figure 10.4C). Figure 10.4A shows the *ITV* evolution at one of the poles of the cell. It can be observed that for the field amplitudes more than 800 V/cm, the membrane capacitor charging shows a nonlinear behavior. Figure 10.4B demonstrates spatial *ITV* over the cell membrane at the end of 100 μs pulses of different pulse strength. The stronger the pulse, the steeper is the conductivity changes (Figure 10.3A), so that *ITV* does not exceed a certain value (Figure 10.4B) except at initial peak overshoot. Figure 10.4C displays the *ITV* distribution on the cell membrane for a 1000 V/cm and 100 μs pulse at times 1, 2, and 100 μs. It can be observed that at the beginning, a dip for *ITV* is created at the poles, which however flattens out with time.

10.4.4 Membrane Permeability

The permeability of the membrane during the pulse in our model is attributed only to P2 pores that are formed during and close after the pulse (Figure 10.5A). After the pulse, the permeability of membrane starts to decrease (Equation 10.11) due to the P2 pores closure and disappearance of endocytosis-like transport (Neumann et al. 1998). Figure 10.5B shows membrane permeability after the pulses that depends strongly on the field strength and pulse duration.
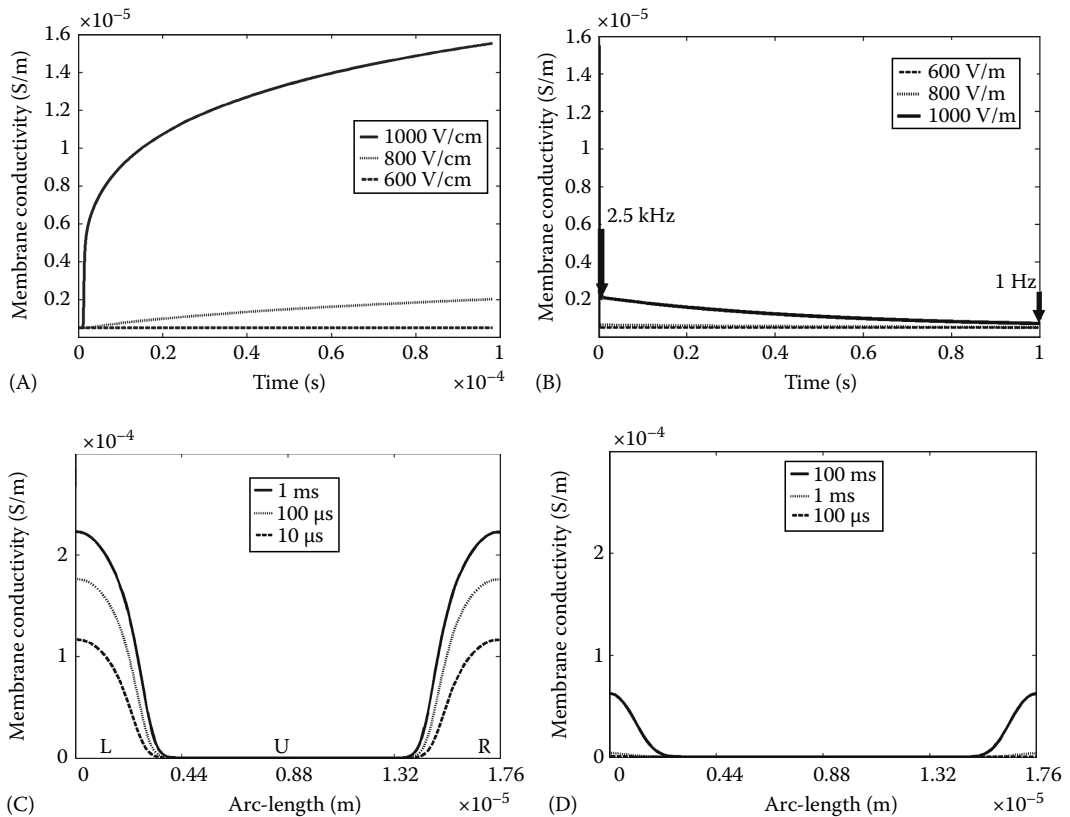
FIGURE 10.3 Temporal and spatial behavior of membrane conductivity. Temporal evolution of the overall membrane conductivity (A) during and (B) after a single 100 μs pulse of different amplitudes 600, 800, and 1000 V/cm. The arrows show the times at which the second pulse of the train pulses with frequencies 2.5 kHz and 1 Hz is to be applied. Spatial distribution of membrane conductivity at the end of (C) a 1000 V/cm pulse of durations 10 μs, 100 μs, and 1 ms and (D) a 700 V/cm pulse of 100 μs, 1 ms, and 100 ms. The right pole, left pole, and the upper equator are indicated by R, L, and U, respectively.

10.4.5 Number of Internalized Molecules to the Cell

The cellular uptake of marker molecule or chemotherapeutic agents is a determinant factor in the efficiency of electroporation-based applications. The results on the number of molecules internalized by the cells with respect to the pulse amplitude and duration, number of pulses, and pulse-repetition frequency are presented.

10.4.5.1 Effect of Pulse Strength and Duration

As Figure 10.6A displays, the amplitude of pulses significantly affects the internalization of molecules, which almost stops at about 16 min after the pulse. It can be seen from the figure that 600 V/cm pulse has no observable effect on the molecular uptake. The effect of pulse duration on the uptake however is not as strong as the influence of pulse amplitude. Figure 10.6B shows the differences in uptake for 1 ms and 100 μs pulses as a function of pulse strength.

10.4.5.2 Effect of Pulse Fractionation (Multiple-Pulse Protocols)

In Figure 10.7A, the uptake of molecules after the exposure of cells to a single 1 ms pulse of 800 V/cm is displayed by a dashed-line curve and the uptake after the fractionation of the pulses to 10 pulses with a duration of 100 μs and frequency of 1 Hz are shown in solid line for each subsequent pulse.
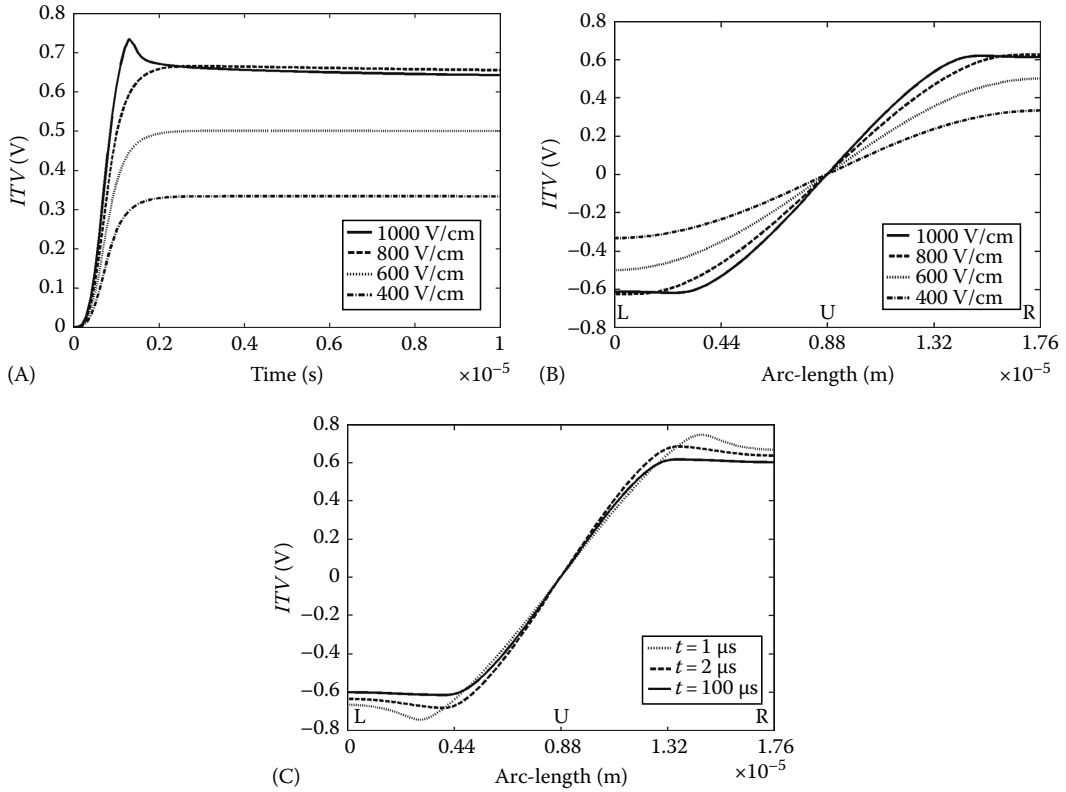
FIGURE 10.4 Temporal and spatial behavior of *ITV*. (A) Time evolution of *ITV* at the left pole (L) for a 100 μs pulse of amplitudes 400, 600, 800, and 1000 V/cm. (B) Spatial distribution of *ITV* on the cell membrane at the end of 100 μs pulses with the same pulse amplitudes of part (A). (C) Spatial distribution of *ITV* for a 1000 V/cm pulse demonstrated at 1, 2, and 100 μs after the pulse starts. The right pole, left pole, and the upper equator are indicated by R, L, and U, respectively.
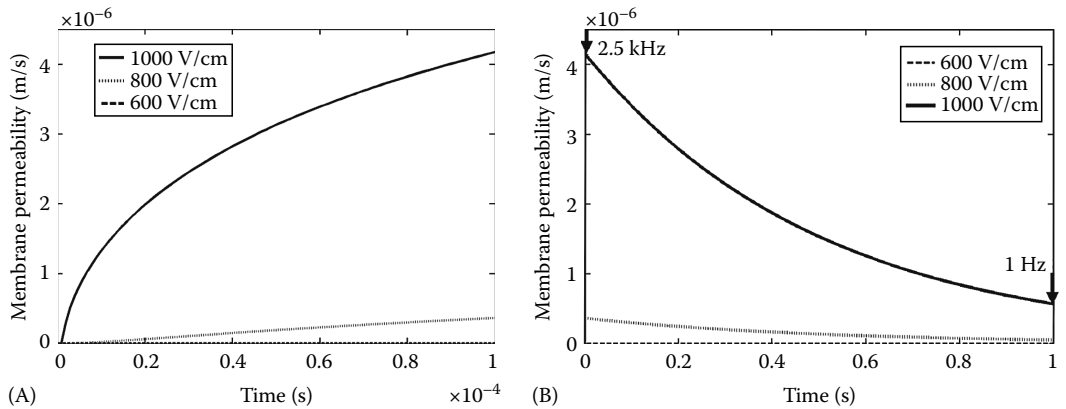

FIGURE 10.5 Temporal evolution of membrane permeability. Temporal evolution of the overall membrane permeability (A) during and (B) after a single 100 μs pulse of different amplitudes 600, 800, and 1000 V/cm. The arrows show the times at which the second pulse of the train pulses with frequencies 2.5 kHz and 1 Hz is to be applied.
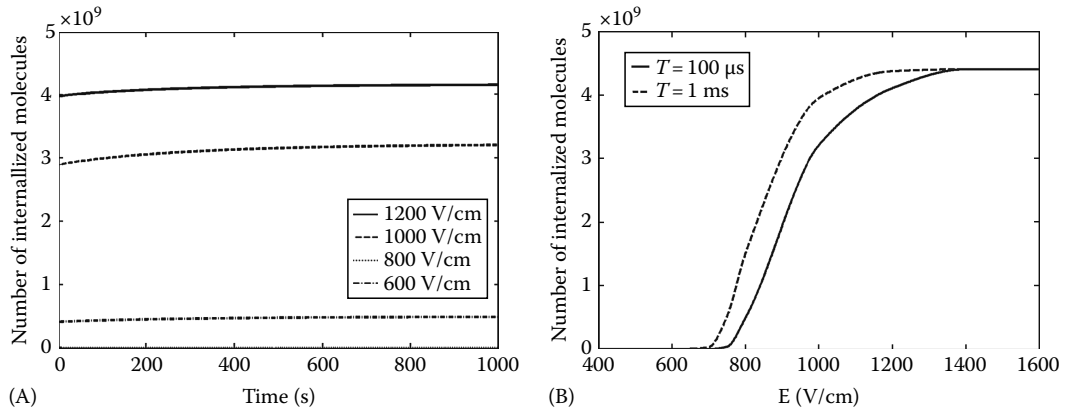
FIGURE 10.6 Dependence of uptake to pulse amplitude and duration. (A) Time evolution of molecule uptake in 16 min after pulse turn-off. Four different pulse amplitudes of 600, 800, 1000, and 1200 V/cm with the same duration of 100 μs are considered. (B) Electric-field amplitude dependence of molecule uptake, 16 min after pulse cessation for two different pulse durations of 100 μs and 1 ms.
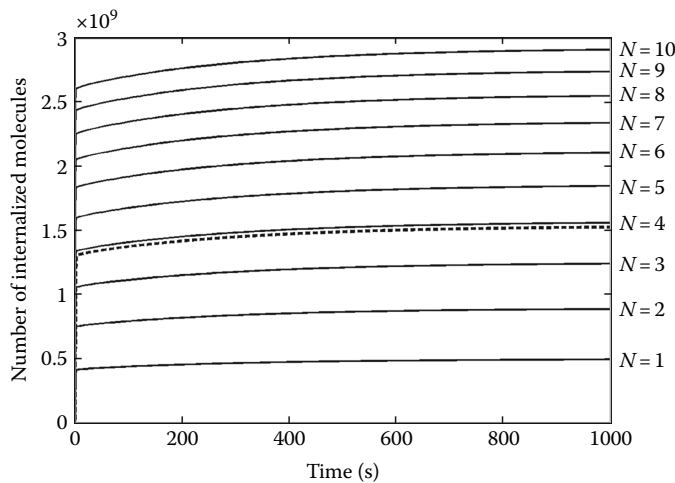

FIGURE 10.7 Dependence of uptake to pulse fractionation. Effect of pulse fractionation. The dashed line demonstrates the uptake due to a single pulse with 800 V/cm amplitude and 1 ms duration. The solid lines indicate the uptake after fractionation of pulsing to 10 pulses of the same amplitude with duration of 100 μs and frequency of 1 Hz. *N* displays the number of pulses.

This difference in the internalization of molecules after the exposure of cells to single and multiple pulses is attributed to the sharp increase of permeability at the beginning of each pulse followed by a smooth increase (Figure 10.5A).

10.4.5.3 Effect of Pulse Frequency and Number of Pulses

There are two distinct factors that need to be taken into account when considering the effect of pulse repetition frequency on molecular uptake: (1) membrane conductivity and (2) the level of membrane permeability, at the start of each consecutive pulse in the pulse train.

In our simulations, we considered 1 Hz and 2.5 kHz pulse-repetition frequency for which the time interval between subsequent pulses is 1 s and 400 μs, respectively. The arrows in Figures 10.3B and 10.5B show the time at which the second pulse of considered pulse repetition frequency is applied. It is evident
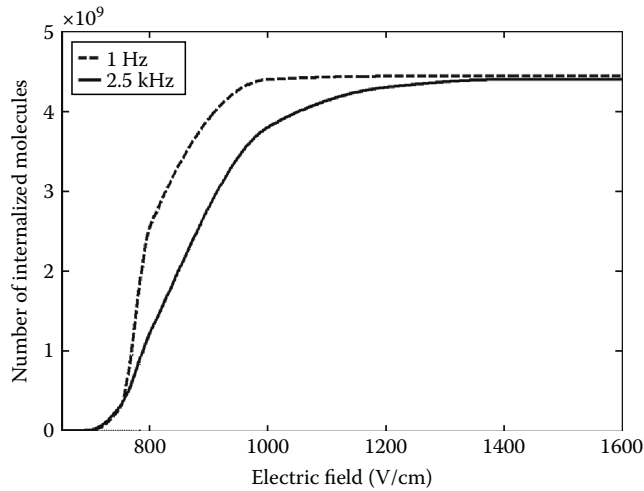
FIGURE 10.8 Dependence of uptake to pulse repetition frequency. Comparison of effectiveness for two trains of pulses consisting of eight pulses with 100 μs duration and 1 Hz and 2.5 kHz frequencies for different pulse strengths.

from Figure 10.3B that when a sequence of pulses is applied, residual membrane conductivity from the preceding pulses results in the lower *ITV* of the cell membrane and subsequently less uptake increase. This leads us to conclude that pulses with higher pulse-repetition frequency are less efficient. That is, for certain electric field strength, the number of internalized molecules for lower pulse-repetition frequency is higher than the related number of internalized molecules for higher frequency. Besides that, the cell membrane appears to be at different states of permeabilization at the beginning of each consecutive pulse based on Figure 10.5B. It can be stipulated that the higher the pulse-repetition frequency, the larger the permeability of the membrane when the next pulse is to be applied. This factor is not as effective as the first one. Figure 10.8 shows the molecular uptake for two pulse-repetition frequencies considered 1 Hz and 2.5 kHz for different pulse amplitudes, which demonstrates that with increasing pulse-repetition frequency, the uptake of subsequent pulses decreases.

10.5 Discussion

The focus of this modeling was to study the effect of electric pulse, duration of exposure, number of pulses, and pulse-repetition frequency on molecular transport using a self-consistent model based on previously proposed chemical-kinetics electroporation scheme. At the same time, the described model enables the determination and prediction of *ITV*, membrane conductivity, and permeability temporarily and spatially for single and multiple electroporation pulse protocols.

   Among different theoretical models for electroporation, some are well established such as resistive-capacitive model, electromagnetic bulk model, and energy models. In the resistive–capacitive (RC) transport lattices (Gowrishankar and Weaver 2003, Stewart et al. 2004), determining the spatial distribution of *ITV* over the cell membrane and the dynamical behavior of the membrane after the breakdown, however, is not possible. In electromagnetic bulk model, the Laplace equation is used to determine the *ITV* (Kotnik et al. 1997). Although with this model spatial distribution is available, it only shows which regions undergo electroporation, and does not consider the variations of *ITV* after electroporation occurs. One of the frequently used models for electroporation is based on Smoluchowski equation together with pore creation energy definition (DeBruin and Krassowska 1999, Neu and Krassowska 1999) in which pores growth and shrinkage (Joshi et al. 2002, 2004, Smith et al. 2004) and self-consistency (Krassowska and Filev 2007) can be taken into account, but it is not applicable to different cell shapes and pulse waveforms. Finally, there is also a model in which conductivity increase due to

electroporation is defined by relations based on experimental findings (Hibino et al. 1993, Pavlin et al. 2005). Other models that allow the prediction of molecular uptake by the cells based on electroporation were also published. A study has been performed on a model for molecules transported after the pulse ends (Pliquett and Weaver 2007). Moreover, a model of diffusion-driven transmembrane transport has been constructed using a pharmacokinetic model (Puc et al. 2003). None of the above-mentioned models however deals with the dynamic behavior and conductivity changes of the cell membrane during and after the pulses and molecular transport through the membrane at the same time.

In a chemical-kinetics model (Böckmann et al. 2008, Neumann et al. 1998), a number of closed and porous states were introduced in order to match the experimental results, and the equations were obtained based on electrochemical considerations so that the pore formation and resealing of the membrane and also molecule uptake can be predicted considering the angular and time average of the parameters (Neumann et al. 1996, 1998, 1999). These models are only suitable for spherical cells and the distribution of pores in the electroporated regions from which the whole transport took place was assumed uniform. Besides, the dynamic behavior of other parameters such as *ITV* and membrane conductivity and permeability has not been considered.

In electroporation experiments, a wide range of resealing times has been reported. It has been observed practically that the electroporated cells continue to take up molecules for minutes and even hours after the pulse, while the membrane conductivity measurements have demonstrated very short time constants (about seconds). Regarding this observation, together with the experimental observations of vesicles during uptake at different times after the pulse (Glogauer et al. 1993, Rols et al. 1995, Zimmermann et al. 1990), we made our model based on the suggestion that all the molecular uptake does not occur through the open pores P2. Rather, we suggest two distinct mechanisms to be involved in transmembrane molecular transport: interactive diffusion through the pores and endocytosis-like transport trough the perturbed area characterized by increased membrane permeability (Equation 10.11).

Our results show that the structural changes of the membrane start at the beginning of the pulse and form continuously. The pore formations are considerable only if the electric field is high enough, which is in agreement with experimental observations (Kotnik et al. 2000, Teissié and Ramos 1998). Therefore, membrane conductivity and permeability change from the very beginning of the pulse, but only become detectable at large-enough electric-field amplitudes (Figure 10.3A). This is in accordance with apparent threshold reported in different experimental studies and should thus be considered as a detectability threshold (Gabriel and Teissié 1999, Kotnik et al. 2000, Rols and Teissié 1990). Even for smaller electric-field amplitudes, increasing the pulse duration may change the electroporation state from undetectable to detectable (Figure 10.3D). This has been observed in experiments but quite commonly explained as a decrease of the threshold transmembrane voltage by increasing the duration of pulses (Canatella et al. 2001, Gowrishankar et al. 1999, Pucihar et al. 2006, 2008). In addition, the obtained temporal and spatial variation of *ITV* (Figure 10.4) is in accordance with experimental observations (Hibino et al. 1993).

According to our model, after the pulse, membrane conductivity decreases based on pore's closure, while increased membrane permeability still allows marker molecules or drugs to be transported through the perturbed area of the membrane. Based on our results (and in agreement with experimental observations (Kotnik et al. 2003, Miklavčič et al. 2000, Puc et al. 2003, Pucihar et al. 2007, He et al. 2007)), the number of internalized molecules to the cell increases with pulse amplitude and duration (Figure 10.6). Another factor that appeared to be important in molecule uptake is the concentration gradient of the molecule at the time of pulse application (data not shown). One important result of our study, which is in line with the experiments and was confirmed by experiments (Hibino et al. 1991), is the description of pulse fractionation effectiveness in molecular uptake for multi-pulse protocols (Figure 10.7). At the same time, our results show that molecular uptake depends on pulse-repetition frequency. Besides, it was shown (Figure 10.6B) that the number of pulses can significantly affect the pulse uptake but only before reaching the saturation, which depends on field strength (Figure 10.6A) and pulse-repetition frequency (Figure 10.8). This has also been observed in previously published experimental studies (Rols and Teissié 1990). However,

in experimental results, at large electric field strengths, the molecule uptake decreases due to irreversible electroporation (Kotnik et al. 2003, 2007). As in our model, irreversible permeabilization was not taken into account, and this decrease cannot be observed in the graphs.

Therefore, using the presented self-consistent model based on chemical-kinetics scheme, we can explain and predict the effect of all pulse parameters, i.e., amplitude, duration, pulse-repetition frequency, and pulse shape. Namely, in our model we can apply realistic pulse shapes and waveforms and also realistic cell geometry.

To have a precise description of molecular transport using this model for different molecules, we need, however, to determine molecular-specific parameters from experiments. Namely, for each different molecule having different size and charge and characteristics, we would need to determine corresponding diffusion coefficients. In our model, we considered uncharged molecules for transport through the membrane. For the macromolecules and highly charged molecules, the electrophoresis however also applies and becomes important in the observed molecular uptake. Thus, the mechanism for the uptake during the pulse is electro-diffusion. Also, in this study, resting transmembrane voltage was considered negligible with respect to *ITV*. These can both be easily introduced in our model and can thus be considered in our future development of this model.

Acknowledgments

References

Abidor IG, Arakelyan VB, Chernomordik LV, Chizmadzhev YA, Pastushenko VF, Tarasevich MR. 1979. Electrical breakdown of BLM: Main experimental facts and their qualitative discussion. *Bioelectrochem Bioenerg* 6:37–52.

Bier M. 2002. Resealing dynamics of a cell membrane after electroporation. *Phys Rev E* 66:062905.

Böckmann RA, Groot BL, Kakorin S, Neumann E, Grubmüller H. 2008. Kinetics, statistics, and energetics of lipid membrane electroporation studied by molecular dynamics simulations. *Biophys J* 95(4):1837–1850.

Canatella PJ, Karr JF, Petros JA, Prausnitz MR. 2001. Quantitative study of electroporation-mediated molecular uptake and cell viability. *Biophys J* 80(2):755–764.

Chernomordik LV, Sukharev SI, Popov SV, Pastushenko VF, Sokirko AV, Abidor IG, Chizmadzhev YA. 1987. The electrical breakdown of cell and lipid membranes: The similarity of phenomenologies. *Biochim Biophys Acta* 902(3):360–373.

Chernomordik LV, Vogel SS, Sokoloff A, Onaran HO, Leikina EA, Zimmerberg J. 1993. Lysolipids reversibly inhibit Ca^{2+}-, GTP- and pH-dependent fusion of biological membranes. *FEBS Lett* 318:71–76.

DeBruin KA, Krassowska W. 1999. Modeling electroporation in a single cell. II. Effects of ionic concentrations. *Biophys J* 77(3):1225–1233.

Escoffre JM, Dean DS, Hubert M, Rols MP, Favard C. 2007. Membrane perturbation by an external electric field: A mechanism to permit molecular uptake. *Eur Biophys J* 36(8):973–983.

Gabriel B, Teissié J. 1999. Time courses of mammalian cell electropermeabilization observed by millisecond imaging of membrane property changes during the pulse. *Biophys J* 76:2158–2165.

Gehl J, Mir LM. 1999. Determination of optimal parameters for in vivo gene transfer by electroporation, using a rapid in vivo test for cell permeabilization. *Biochem Biophys Res Commun* 261(2):377–380.

Ghosh PM, Keese CR, Giaever I. 1993. Monitoring electropermeabilization in the plasma membrane of adherent mammalian cells. *Biophys J* 64:1602–1609.

Glaser RW, Wagner A, Donath E. 1986. Volume and ionic composition changes in erythrocytes after electric breakdown—Simulation and experiment. *Bioelectrochem Bioenerg* 16:455–467.

Glaser RW, Leikin SL, Chernomordik LV, Pastushenko VF, Sokirko AI. 1988. Reversible electrical breakdown of lipid bilayers: Formation and evolution of pores. *Biochim Biophys Acta* 940:275–287.

Glogauer M, Lee W, McCulloch CA. 1993. Induced endocytosis in human fibroblasts by electrical fields. *Exp Cell Res* 208(1):232–240.

Gowrishankar TR, Weaver JC. 2003. An approach to electrical modeling of single and multiple cells. *Proc Natl Acad Sci USA* 100(6):3203–3208.

Gowrishankar TR, Pliquett U, Lee RC. 1999. Dynamics of membrane sealing in transient electropermeabilization of skeletal muscle membranes. *Ann NY Acad Sci* 888:195–210.

He H, Chang DC, Lee YK. 2007. Using a micro electroporation chip to determine the optimal physical parameters in the uptake of biomolecules in HeLa cells. *Bioelectrochemistry* 70:363–368.

He H, Chang DC, Lee YK. 2008. Nonlinear current response of micro electroporation and resealing dynamics for human cancer cells. *Bioelectrochemistry* 72(2):161–168.

Hibino M, Shigemori M, Itoh H, Nagayama K, Kinosita K. 1991. Membrane conductance of an electroporated cell analyzed by submicrosecond imaging of transmembrane potential. *Biophys J* 59:209–220.

Hibino M, Itoh H, Kinosita K. 1993. Time courses of cell electroporation as revealed by submicrosecond imaging of transmembrane potential. *Biophys J* 64:1789–1800.

Jones AT. 2007. Macropinocytosis: Searching for an endocytic identity and role in the uptake of cell penetrating peptides. *J Cell Mol Med* 11(4):670–684.

Joshi RP, Hu Q, Schoenbach KH, Bebe SJ. 2002. Simulations of electroporation dynamics and shape deformations in biological cells subjected to high voltage pulses. *IEEE Trans Plasma Sci* 30:1536–1546.

Joshi RP, Hu Q, Schoenbach KH. 2004. Modeling studies of cell response to ultrashort, high-intensity electric fields—Implications for intracellular manipulation. *IEEE Trans Plasma Sci* 32:1677–1686.

Kakorin S, Neumann E. 2002. Ionic conductivity of electroporated lipid bilayer membranes. *Bioelectrochemistry* 56:163–166.

Kakorin S, Stoylov SP, Neumann E. 1996. Electro-optics of membrane electroporation in diphenylhexatriene-doped lipid bilayer vesicles. *Biophys Chem* 16;58(1–2):109–116.

Khine M, Zanetti CI, Blatz A, Wang LP, Lee LP. 2007. Single-cell electroporation arrays with real-time monitoring and feedback control. *Lab Chip* 7:457–462.

Kinosita K Jr, Ikegami A. 1988. A dynamic structure of membranes and subcellular components revealed by optical anisotropy decay method. *Subcell Biochem* 13:55–88.

Kotnik T, Bobanovic F, Miklavcic D. 1997. Sensitivity of transmembrane voltage induced by applied electric fields—A theoretical analysis. *Bioelectrochem Bioenerg* 43:285–291.

Kotnik T, Miklavcic D, Slivnik T. 1998. Time course of transmembrane voltage induced by time-varying electric fields—A method for theoretical analysis and its application. *Bioelectrochem Bioenerg* 45:3–16.

Kotnik T, Macek-Lebar A, Miklavcic D, Mir LM. 2000. Evaluation of cell membrane electropermeabilization by means of nonpermanent cytotoxic agent. *Biotechniques* 28:921–926.

Kotnik T, Pucihar G, Rebersek M, Mir LM, Miklavcic D. 2003. Role of pulse shape in cell membrane electropermeabilization. *Biochim Biophys Acta* 1614:193–200.

Krassowska W, Filev PD. 2007. Modeling electroporation in a single cell. *Biophys J* 92:404–417.

Lambert H, Pankov R, Gauthier J, Hancock R. 1990. Electroporation-mediated uptake of proteins into mammalian cells. *Biochem Cell Biol* 68:729–734.

Miklavcic D, Semrov D, Mekid H, Mir LM. 2000. A validated model of in vivo electric field distribution in tissues for electrochemotherapy and for DNA electrotransfer for gene therapy. *Biochim Biophys Acta* 1523:73–83.

Navarrete EG, Sacchi JS. 2006. On the effect of prestin on the electrical breakdown of cell membranes. *Biophys J* 90(3):967–974.

Neu JC, Krassowska W. 1999. Asymptotic model of electroporation. *Phys Rev E* 59:3471–3482.

Neumann E, Rosenheck K. 1972. Permeability changes induced by electric impulses in vesicular membranes. *J Membr Biol* 10(3):279–290.

Neumann E, Kakorin S, Tsoneva I, Nikolova B, Tomov T. 1996. Calcium-mediated DNA adsorption to yeast cells and kinetics of cell transformation by electroporation. *Biophys J* 71:868–877.

Neumann E, Toensing K, Kakorin S, Budde P, Frey J. 1998. Mechanism of electroporative dye uptake by mouse B cells. *Biophys J* 74(1):98–108.

Neumann E, Kakorin S, Toensing K. 1999. Fundamentals of electroporative delivery of drugs and genes. *Bioelectrochem Bioenerg* 48:3–16.

Pavlin M, Kanduser M, Rebersek M, Pucihar G, Hart FX, Magjarevic R, Miklavcic D. 2005. Effect of cell electroporation on the conductivity of a cell suspension. *Biophys J* 88:4378–4390.

Pavlin M, Leben V, Miklavcic D. 2007. Electroporation in dense cell suspension—Theoretical and experimental analysis of ion diffusion and cell permeabilization. *Biochim Biophys Acta* 1770:12–23.

Pliquett U, Weaver JC. 2007. Feasibility of an electrode-reservoir device for transdermal drug delivery by noninvasive skin electroporation. *IEEE Trans Biomed Eng* 54:536–538.

Plonsey R, Barr RC. 1988. *Bioelectricity. A Quantitative Approach*. New York, Plenum Press.

Prausnitz MR, Corbett JD, Gimm JA, Golan DE, Langer R, Weaver JC. 1995. Millisecond measurement of transport during and after an electroporation pulse. *Biophys J* 68(5):1864–1870.

Puc M, Kotnik T, Mir LM, Miklavcic D. 2003. Quantitative model of small molecules uptake after in vitro cell electropermeabilization. *Bioelectrochemistry* 60:1–10.

Pucihar G, Mir LM, Miklavcic D. 2002. The effect of pulse repetition frequency on the uptake into electropermeabilized cells in vitro with possible applications in electrochemotherapy. *Bioelectrochemistry* 57:167–172.

Pucihar G, Kotnik T, Valic B, Miklavcic D. 2006. Numerical determination of transmembrane voltage induced on irregularly shaped cells. *Ann Biomed Eng* 34:642–652.

Pucihar G, Kotnik T, Teissié J, Miklavcic D. 2007. Electroporation of dense cell suspensions. *Eur Biophys J* 36:173–185.

Pucihar G, Kotnik T, Miklavcic D, Teissié J. 2008. Kinetics of transmembrane transport of small molecules into electropermeabilized cells. *Biophys J* 95:2837–2848.

Rols MP, Teissié J. 1990. Electropermeabilization of mammalian cells. *Biophys J* 58:1089–1098.

Rols MP, Teissié J. 1998. Electropermeabilization of mammalian cells to macromolecules: Control by pulse duration. *Biophys J* 75:1415–1423.

Rols MP, Femenia P, Teissié J. 1995. Long-lived macropinocytosis takes place in electropermeabilized mammalian cells. *Biochem Biophys Res Commun* 208:26–38.

Ryttsén F, Farre C, Brennan C, Weber SG, Nolkrantz K, Jardemark K, Chiu DT, Orwar O. 2000. Characterization of single-cell electroporation by using patch-clamp and fluorescence microscopy. *Biophys J* 79(4):1993–2001.

Saulis G. 1997. Pore disappearance in a cell after electroporation: Theoretical simulation and comparison with experiments. *Biophys J* 73(3):1299–1309.

Saulis G. 2005 The loading of human erythrocytes with small molecules by electroporation. *Cell Mol Biol Lett* 10:23–35.

Saulis G, Venslauskas MS, Naktinis J. 1991. Kinetics of pore resealing in cell membranes after electroporation. *Bioelectrochem Bioenerg* 26:1–13.

Saulis G, Satkauskas S, Praneviciute R. 2007. Determination of cell electroporation from the release of intracellular potassium ions. *Anal Biochem* 360(2):273–281.

Schmeer M, Seipp T, Pliquett U, Kakorin S, Neumann E. 2004. Mechanism for the conductivity changes caused by membrane electroporation of CHO cell—pellets. *Phys Chem Chem Phys* 6:5564–5574.

Schwister K, Deuticke B. 1985. Formation and properties of aqueous leaks induced in human erythrocytes by electrical breakdown. *Biochim Biophys Acta* 816:332–348.

Shirakashi R, Sukhorukov VL, Tanasawa I, Zimmermann U. 2004. Measurement of the permeability and resealing time constant of the electroporated mammalian cell membranes. *Int J Heat Mass Transfer* 47(21):4517–4524.

Smith KC, Neu JC, Krassowska W. 2004. Model of creation and evolution of stable electropores for DNA delivery. *Biophys J* 86:2813–2826.

Sowers AE. 1986. A long-lived fusogenic state is induced in erythrocytes ghosts by electric pulses. *J Cell Biol* 102:1358–1362.

Stewart DA Jr, Gowrishankar TR, Weaver JC. 2004. Transport lattice approach to describing cell electroporation: Use of a local asymptotic model. *IEEE Trans Plasma Sci* 32(4):1696–1708.

Teissié J, Ramos C. 1998. Correlation between electric field pulse induced long-lived permeabilization and fusogenicity in cell membranes. *Biophys J* 74(4):1889–1898.

Teissié J, Golzio M, Rols MP. 2005. Mechanisms of cell membrane electropermeabilization: A mini review of our present (lack of?) knowledge. *Biochim Biophys Acta* 1724(3):270–280.

Tsong TY. 1991. Electroporation of cell membranes. *Biophys J* 60:297–306.

Weaver JC, Chizmadzhev YA. 1989. Theory of electroporation: A review. *Bioelectrochem Bioenerg* 41:135–160.

Zimmermann U. 1982. Electric field-mediated fusion and related electrical phenomena. *Biochim Biophys Acta* 694:227–277.

Zimmermann U, Schnettler R, Klöck G, Watzka H, Donath E, Glaser RW. 1990. Mechanisms of electro-stimulated uptake of macromolecules into living cells. *Naturwissenschaften* 77:543–545.